Electronic Supplementary Material (ESI) for RSC Advances.

The concentration-dependent effect of hydrocortisone on the structure of model lung surfactant monolayer by using an *in-silico* approach

Mohammad Zohurul Islam[1*], Sheikh I. Hossain[2], E. Deplazes[2,a], Zhen Luo[1] and Suvash C. Saha[1, a]

[1]*School of Mechanical and Mechatronic Engineering, University of Technology Sydney, 15 Broadway, Ultimo, NSW 2007, Australia*
[2]*School of Life Sciences, University of Technology Sydney, 15 Broadway, Ultimo, NSW 2007, Australia*

[a] co-corresponding author: Suvash.Saha@uts.edu.au and Evelyne.Deplazes@uts.edu.au

[*] *Current affiliation: Department of Mathematics, Faculty of Science, Jashore University of Science and Technology, Jashore-7408, Bangladesh*

S1.1 Bead types and topology for hydrocortisone

Due to the structural similarity between different corticosteroids, the detailed information about the parameterisation of the hydrocortisone CG model has been given, which are presented in the following Table S1. This is done by the process of small molecules parameterisation from martini website [1]. The bead mapping of hydrocortisone was constructed and presented in Fig. 1b, c in the main text. Based on the corticosteroid drug (prednisolone) structure [2], the CG model for hydrocortisone was structured and standard Martini bead types were used [3]. Once getting the stable CG model of the hydrocortisone, the partitioning free energy was calculated by using umbrella sampling simulation (discussed in supplementary section S1.2 in detail). The partition coefficient (logP value) of hydrocortisone was calculated from the Gibbs free energy difference, and the obtained value was compared with experimental, predicted, and simulated partition coefficient of hydrocortisone to validate the hydrocortisone CG parameter. It is very important to note that since the experimental logP value of hydrocortisone for LSM does not exist in literature so far, hence in this model, the calculated octanol-water partition coefficient (logP) of hydrocortisone was used to validate the parameterisation. The obtained logP value is also compared with predicted logP values at different scale from drug data bank of hydrocortisone as presented in Table S3.

Table S1: Detailed information about the CG model for Hydrocortisone.

Molecule	Group	Atom name	Bead type	Group representation
Hydrocortisone	1	RO1	SNa	Cyclic ketone
	2	R1	SC3	Cyclic alkene
	3	R2	SC2	Cyclic alkane
	4	ROH1	SP1	Cyclic alcohol
	5	R3	SC2	Cyclic alkane
	6	ROH2	SP1	Cyclic alcohol
	7	RO2	SNa	Cyclic ketone
	8	ROH3	P2	Aliphatic alcohol

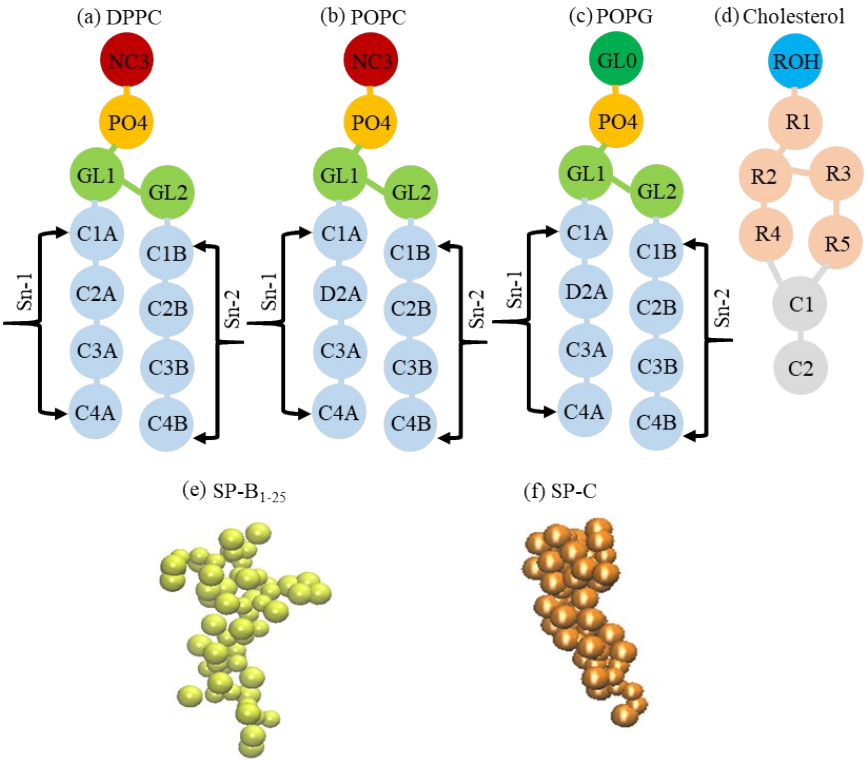

Figure S1. Schematic representation of the CG structure of (a) DPPC, (b) POPC, (c) POPG, (d) cholesterol, (e) surfactant protein B ($SP\text{-}B_{1\text{-}25}$) and (f) surfactant protein C (SP-C).

Table S2: System charges after adding 150 mM NaCl (Na^+ and Cl^- ions) into the water sandwiched between the monolayers.

Components	Number of Molecules/Ions	Charge (e)
SP-B	8	+32
SP-C	8	+24
DPPC	1224	0
POPC	408	0
POPG	200	-200
CHOL	200	0
HCOT (drug)	20/60/120/240	0
Water	47546	0
Na^+	3318	+3318
Cl^-	3174	-3174

S1.2 Umbrella sampling simulation

The free energy profile or potential mean force (PMF) of hydrocortisone from octanol phase (hydrophobic medium) into water (hydrophilic medium) phase was estimated with the help of umbrella sampling (US) technique [4-7]. For partition coefficient calculation, an octanol-water biphasic model was prepared with the box size 5×5×24 nm^3. The simulation system was constructed using two pre-equilibrated water boxes (containing 1470 water molecules each) separated by a pre-equilibrated octanol box (containing 765 octanol molecules) at middle place of the box and maintain the box dimension 5×5×8 nm^3 for each of three boxes. The coarse-grained parameters for octanol was taken from the existing literature [6, 7] and for water from standard Martini force field [3, 8].

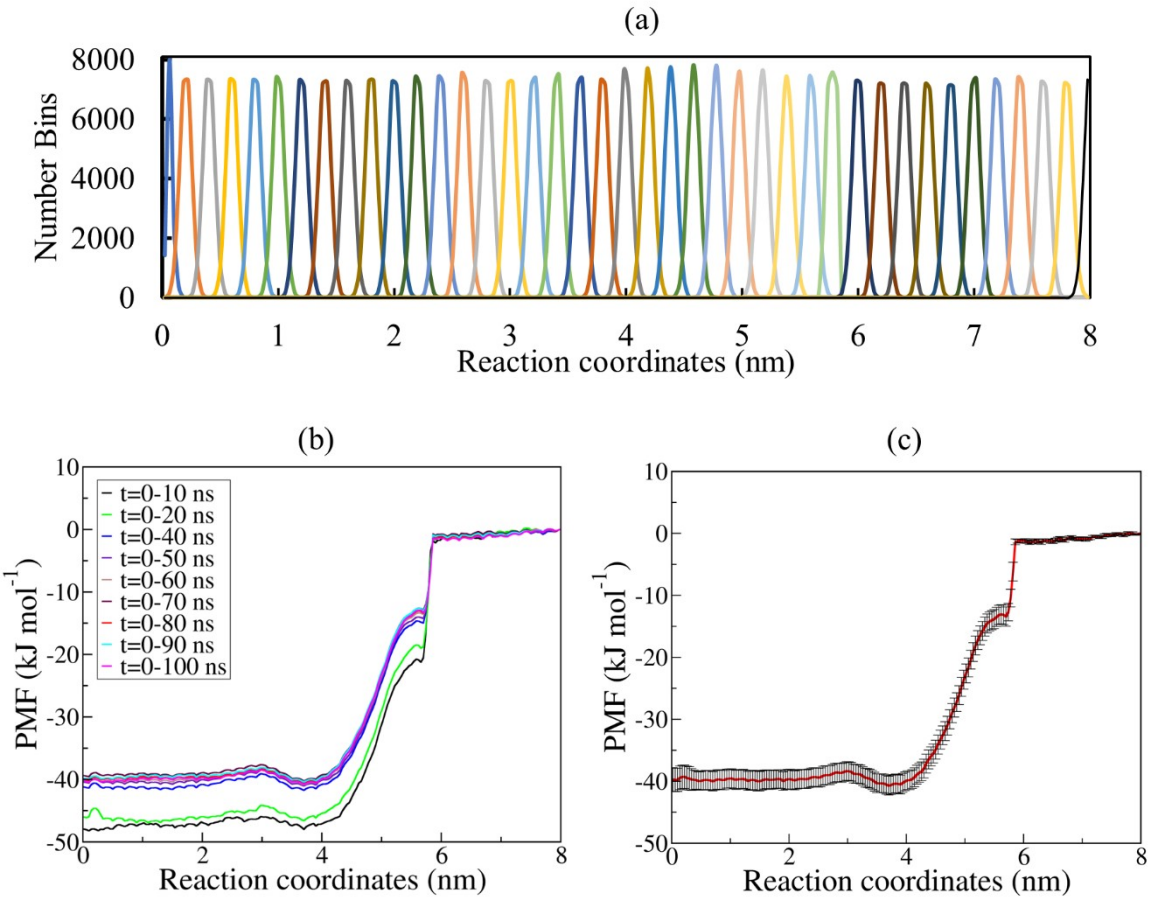

Figure S2. (a) The weighted histogram analysis to check the overlap between umbrella windows along the reaction coordinate (i.e., z-axis) starting from 0 to 8 nm. Free energy profile of hydrocortisone shifted from octanol to water phase. (b) Potential mean force (PMF) calculation at various simulation times for convergence test of the calculation to get the reliable partition coefficient. (c) PMF curve of hydrocortisone transferred from octanol phase to water phase with uncertainties calculated using Bootstrapping analysis.

The simulations were initiated with single hydrocortisone molecule placing into the octanol phase (at center of mass of octanol box). The hydrocortisone molecule was then pulled towards the any side of water phase by ensuring a total travelling distance 8 nm along the reaction coordinates normal to the octanol-water surface (along *z*-axis). The interval between two adjacent initial configuration was 0.2 nm, and a total of 40 windows was considered to pull (8 nm) along the reaction coordinates. The starting configurations of US were then collected from trajectories. In the time of pulling, the distance between the center of mass of the drug and of the solvent is measured by z_i (along *z*-axis only keeping *x*, and *y* direction unchanged) applying a harmonic potential, V_{us} is defined by,

$$V_{us} = \frac{1}{2} k_{us} (z - z_i)^2 \quad (1s)$$

where, K_{us} is the harmonic force constant, the value of this forced constant is varied from 100 to 2000 kJ mol^{-1} nm^{-2} depending on the barrier energy of the octanol-water interface to keep the drug molecule in the reference position. The steepest descent algorithm was applied until the maximum energy gradient smaller than 100 kJ mol^{-1} nm^{-1} to avoid the collisions between drug, water, or octanol molecules [9]. After energy minimisation, an equilibration with NVT ensemble for 50 ns was applied with the velocity rescale thermostat [10] (τ = 1.0 ps) at temperature 298 *K* to get reasonable velocity distribution of the molecules. In order to ensure appropriate density of the system, we performed NPT (constant particle number, pressure and temperature) ensemble for 100 ns using Berendsen pressure coupling [11] (τ = 12.0 ps) at 1.0 *bar* with semi-isotropic pressure and previous thermostat (τ = 1.0 ps) at temperature 298 *K*. Finally, we began production run for 100 ns applying velocity rescale thermostat [10] (τ = 1.0 ps) at temperature 298 *K* and Parrinello-Rahman pressure coupling [12] (τ = 12.0 ps) at 1.0 bar with isotropic pressure and a compressibility 4.5 $\times 10^{-5}$ bar^{-1} was applied. The neighbour list was updated for every 20 steps and the integration time was 20 fs for all simulations [13-15]. The relative dielectric constant was set to 15, as used in the MARTINI force field [16]. The cut-off for Coulomb interaction potential was shifted to zero between 0 and 1.2 nm, whereas the cut-off for Lennard-Jones interaction potential was shifted to zero between 0 and 1.2 nm. The leap-frog algorithm was applied for all the steps [17]. The trajectories were finally collected from MD simulation to calculate potential mean force (Gibbs free energy) over the total 40 umbrella windows spaced by 0.2 nm. Finally, the weighted histogram analysis method (WHAM) [4] was applied to estimate the Gibbs free energy profile Fig S2. The uncertainties were measured with the help of the Bootstrapping analysis method [18, 19] as shown in Fig. S2.

Table S3: Partition coefficient (logP value) of various corticosteroid drug molecules.

Drug Molecules	CG model	Computational	Predicted		Experiment
			ALOGPS [20]	ChemAxon [21]	
Prednisolone	5.79	3.90 (US*) [2] 5.10 (TI$,&) [2]	1.66	1.27	1.62 [22]
Cholesterol	8.72& [15]	16.55# [3, 23] 10.84@ [16] 8.72& [15]	7.02	7.11	3.70 [15, 24, 25]
Mometasone	7.97	-	2.81	3.50	2.10 [26]
Cortisone	5.60	-	1.98	1.66	1.47 [22]
Hydrocortisone	7.01		1.79	1.28	1.61 [22]

* indicates Umbrella Sampling; $ indicates Thermodynamic Integration; & indicates octanol-water logP; @ indicates hexadecane-water logP; #indicates oil-water logP.

S1.3 Drug concentration calculation

The number of drug molecules required to reach the desired drug concentrations is calculated and presented in Table 1 in the main text. This calculation is based on the number of lipids in the system and the relative molecular weights of all system components according to the formula (Eq. 1s). Table 1 represents the monolayer composition and the drug molecules required for achieving drug concentrations from 0.0% to 10.46% w/w.

$$\text{Weight \% of molecules} = \frac{Molecular\ weight\ of\ the\ individual\ molecules}{Total\ weight\ of\ the\ molecules} \times 100\% \quad \text{1s}$$

As outlined below, the number of drugs used in our simulations are comparable to the amount of drug delivered to the lung in a single puff by meter dose inhaler. The calculation is based on the average area of an adult lung, the typical doses of inhaled steroid drugs such as prednisolone, and the known efficiency of puffers used for pulmonary steroid delivery, which is around 50% [27-29].

Typical doses of corticosteroid for inhalation are range from 100 micrograms (low dose) to 2000 micrograms (high dose) for adults. This is usually delivered in 2 daily doses. For our calculations, we use 50 µg as low dose and 1000 µg as high dose. Using Avogadro's number and the molecular weight of prednisolone (362.46 g/mol), the number drug molecules for these doses can be calculated. We then need to take into account the ratio of the lung surfactant components and the composition of our LSM in the simulation system. The total alveolar area is approximately 70 m^2 [30, 31] for an adult lung, the average area of the LSM in our simulations

is 292 nm^2, and thus there are two monolayers giving a total area of 584 nm^2. Using Eq. 2s the number of molecules for 50 µg and 1000 µg are less than 2 molecule and 26 molecules, respectively. If we assume a puffer efficiency of this equates to 1 and 13 molecules that reach the LSM of an area used in our simulations.

$$\text{Number of drug} = \frac{Drug\ dose \times Avogadro's\ number \times LSM\ area\ in\ simulation}{Molecular\ weight \times Total\ aveolar\ area} \quad \text{2s}$$

As noted above, we simulated the LSM in the presence of five different drug concentrations given as % based on the molecular weight of the drugs and the lipid components in the LSM (Eq. 1s). These concentrations equate to 0.49% for 10 drug molecules, 1.44% for 30 drug molecules, 2.84% for 60 drug molecules, 5.52% for 120 drug molecules and 10.46% for 240 drug molecules. The lower drug concentrations used in our simulations are thus comparable to clinically used doses. The higher drug concentrations were used to investigate the effect of high concentration on the LSM.

S1.4 Lipid order parameter calculation

The order parameter of lipids in bilayers or monolayers is a measure of their structural orientation or flexibility. The order parameter of the monolayer phospholipids tail beads can be measured by the following equation (Eq. 3s),

$$S_z = \frac{1}{2}\left(3\langle \cos^2\theta \rangle - 1\right) \quad \text{(3s)}$$

where S_z be the order parameter, θ be the angle between lipid tails and monolayer normal [32], angular brackets specifies the mean of temporal and molecular ensembles [33]. The values of S_z ranging from -0.5 to 1.0 indicating that when $S_z = 1$, then the phospholipids tails are perfectly aligned along parallel to the monolayer normal (along *z*-axis), whereas $S_z = -0.5$ implying that the phospholipids tails are completely anti-align along monolayer normal. In our study, the python script *do-order-gmx5.py* (MARTINI website) is used to calculate order parameter [34]. Order parameter provides information about the phase behavior of the monolayer, and the instabilities of order parameter values suggest that lipids are in a phase transitional state. The higher value of order parameter (*Sz* = 1) refers to the monolayer is in LC phase representing

the highly ordered lipids chains along monolayer normal (*z-axis*) and unlike the lipids in the LE phase.

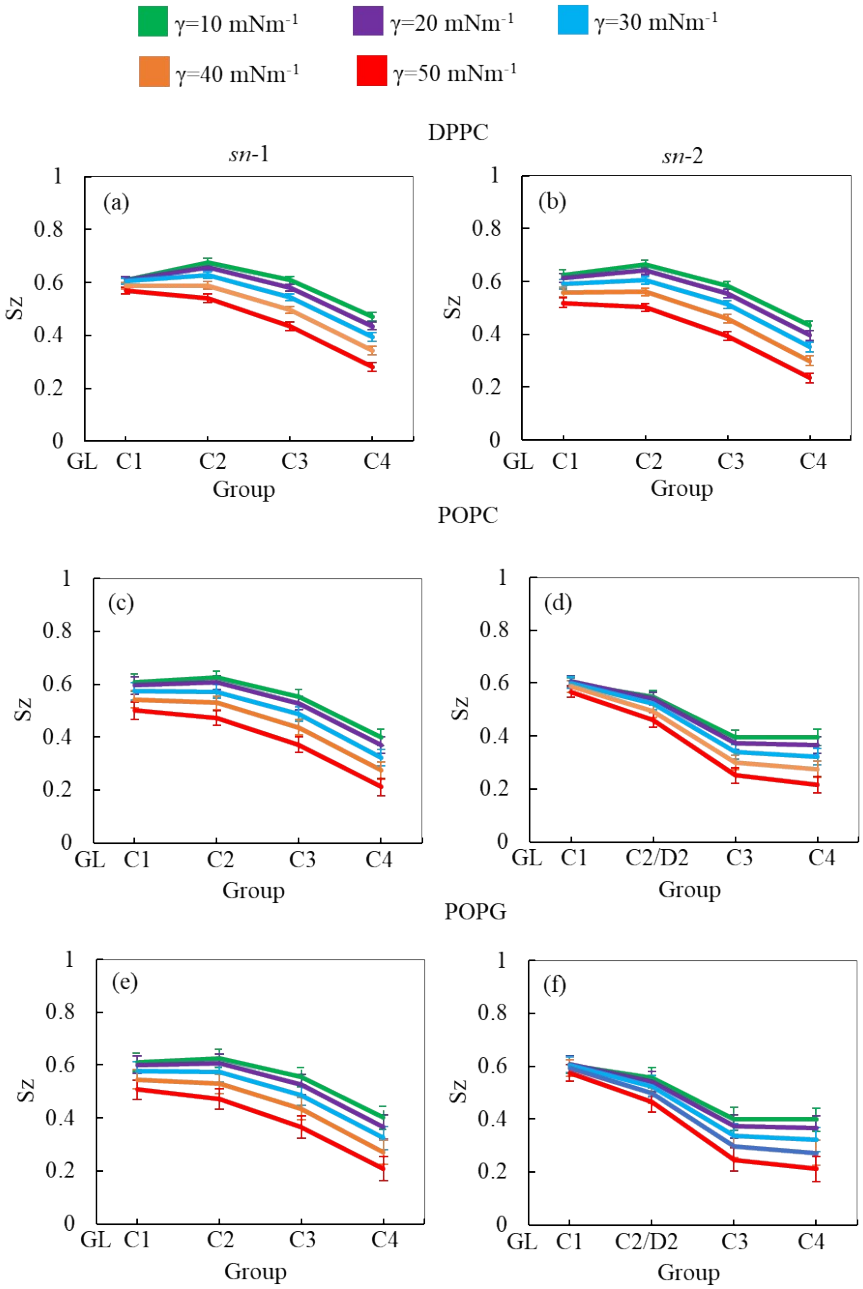

Figure S3. Order parameter of DPPC (a, b), POPC (c, d) and POPG (e, f) for *sn*-1 (a, c, e) and *sn*-2 (b, d, f) chains at different surface tension (0, 10, 20, 30, 40 and 50 mNm^{-1}) in the presence of 5.52% w/w drug containing monolayers composed of DPPC-POPC-POPG-CHOL-SP-B_{1-25}-SP-C. Order parameters were estimated for last one microsecond of the two microsecond simulations. The error bars denote standard deviations across the frames of the trajectories.

Table S4: Monolayer thickness measurement at various surface tension for drug-free monolayer and at 5.52% w/w drug concentration.

Drug concentration (in % w/w)	Surface tension (in mNm^{-1})	Approximate monolayer thickness (in nm)
0	0	2.4
	10	2.4
	20	2.4
	30	2.4
	40	2.4
	50	2.4
5.52	0	-
	10	2.4
	20	2.4
	30	2.4
	40	2.4
	50	2.4

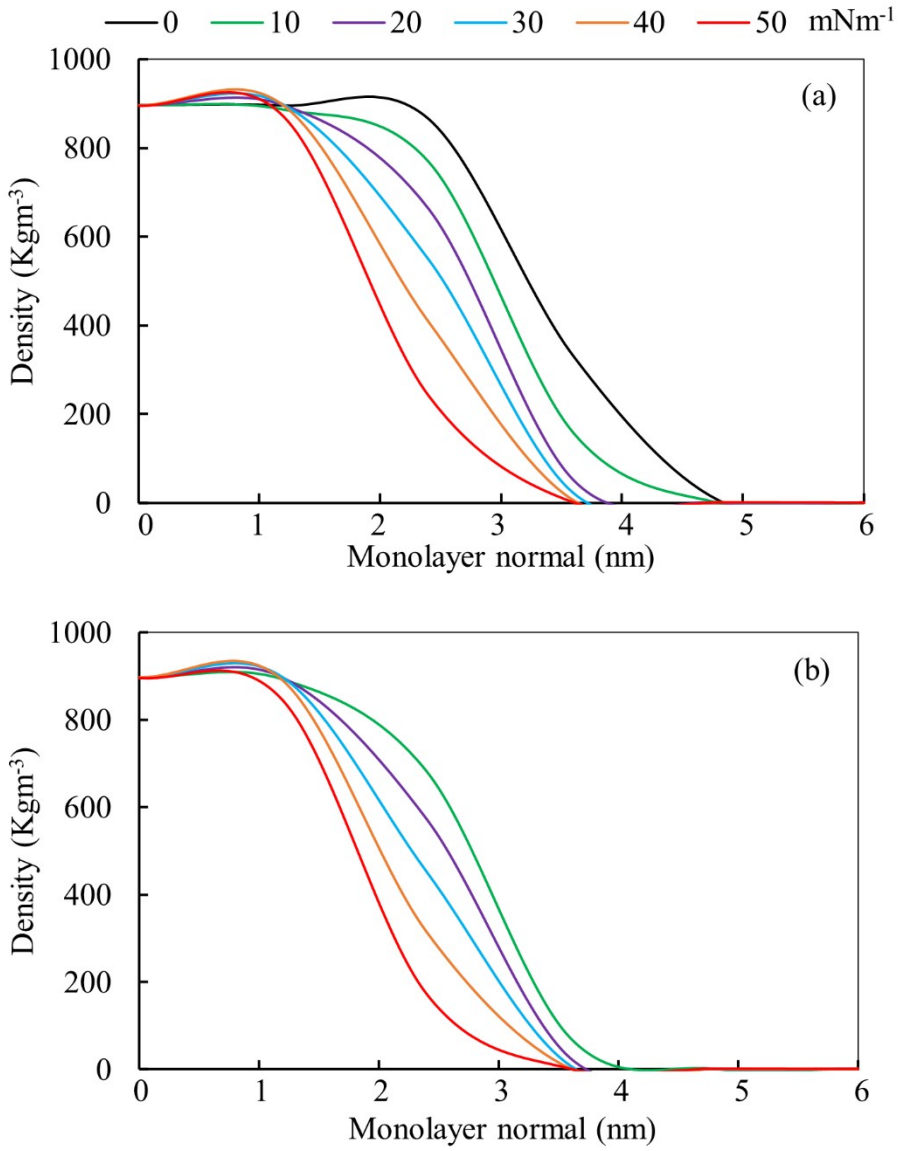

Figure S4. Averaged mass density profiles of water for the LSM composed of DPPC:POPC:POPG:CHOL:SP-$B_{1\text{-}25}$:SP-C. Comparison of density curves of LSM model at different surface tension in the absence (a) and presence (b) of 5.52% w/w hydrocortisone concentration.

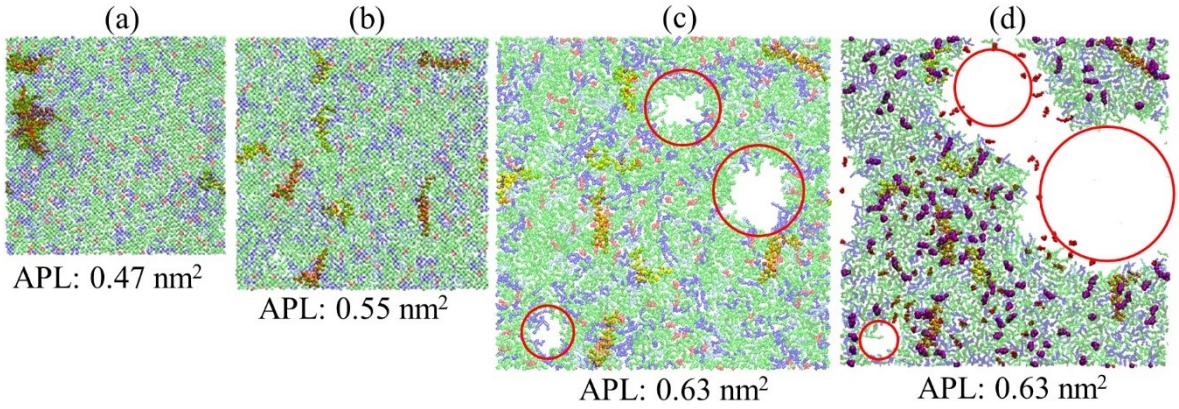

Figure S5. Snapshots of simulation system at (a) APL=0.47 nm^2 (highly compressed monolayer), (b) APL=0.55 nm^2 (intermediate state, i.e., compressed-expanded monolayer), (c) APL=0.63 nm^2 (expanded monolayer) in the absence drug and (d) APL=0.63 nm^2 (expanded monolayer) in the presence of 5.52% w/w drug concentration. Components are shown as DPPC (green), POPC (blue), POPG (cyan), CHOL (red), SP-B_{1-25}(orange), SP-C (yellow) and drug (purple).

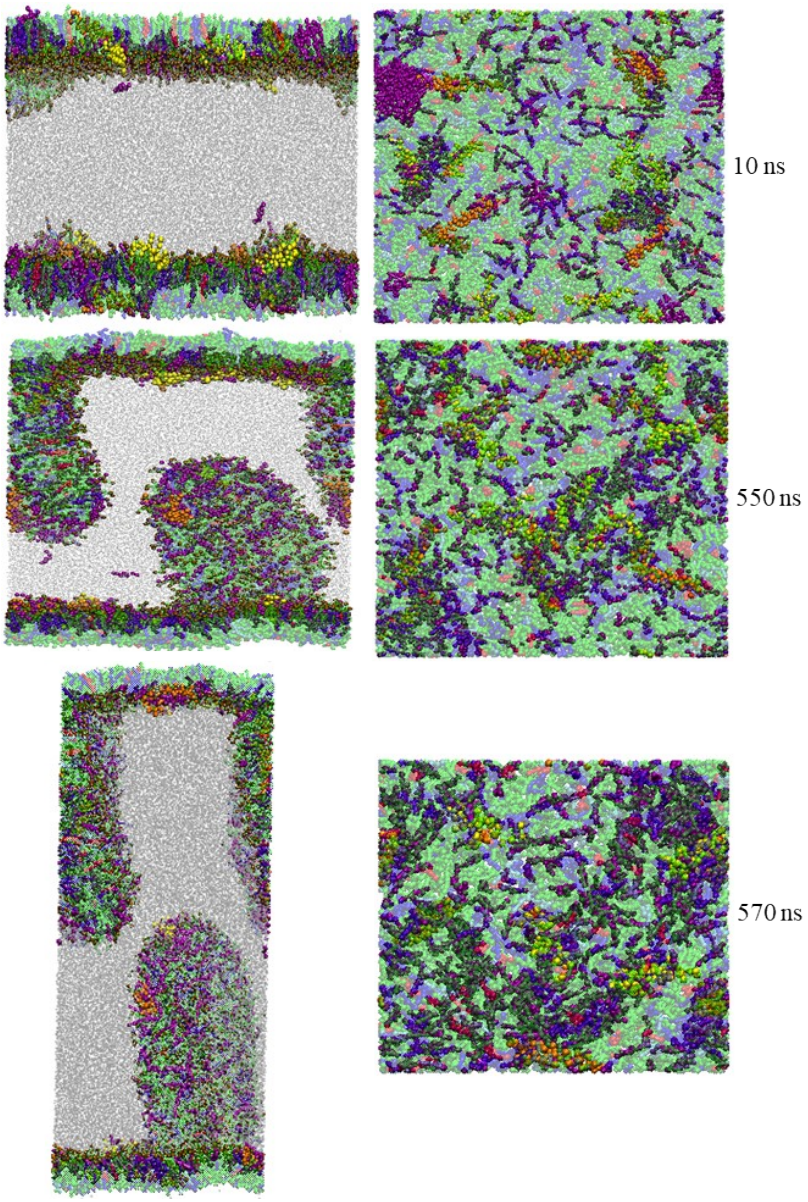

Figure S6. Snapshots of simulation systems for monolayers at surface tension γ=20 mNm^{-1} in the presence of 10.46% w/w hydrocortisone concentrations for the LSM monolayer composed of DPPC-POPC-POPG-CHOL-SP-B_{1-25}-SP-C. DPPC (green), POPC (blue), POPG (cyan), CHOL (red), SP-B_{1-25}(orange), SP-C (yellow), hydrocortisone (purple), water (silver), and phospholipids head groups (ochre).

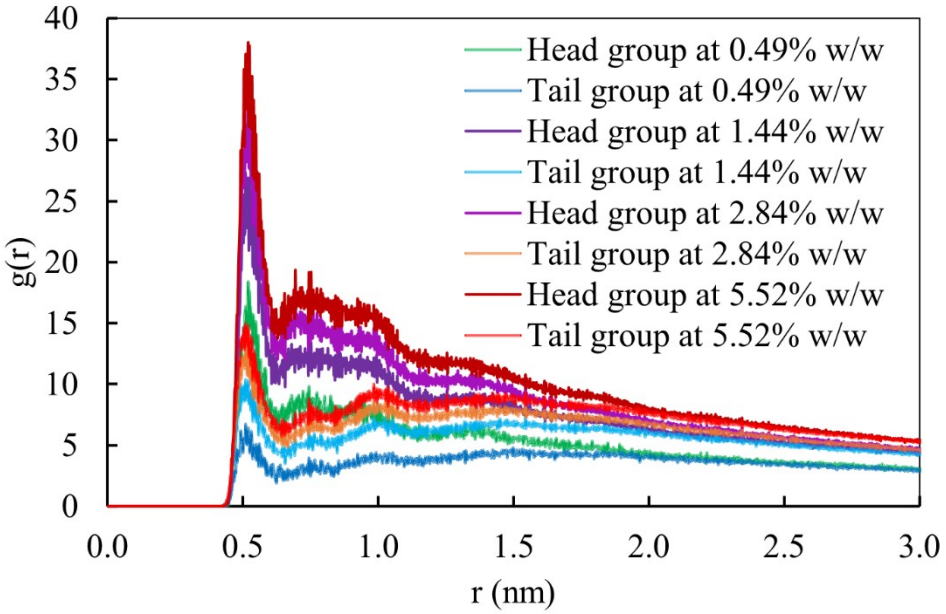

Figure S7. The radial distribution function (RDF) between drug-lipid head group (PO_4) and drug-lipid tail group (hydrophobic lipid chain) at different drug concentrations for the expanded of the monolayer (20 mNm^{-1} surface tension).

References

1. Martini, General Purpose Coarse-Grained Force Field, http://www.cgmartini.nl/index.php/tutorials-general-introduction-gmx5/parametrzining-new-molecule-gmx5, 2020).
2. E. D. Estrada-López, E. Murce, M. P. Franca and A. S. Pimentel, *RSC Advances*, 2017, **7**, 5272-5281.
3. S. J. Marrink, H. J. Risselada, S. Yefimov, D. P. Tieleman and A. H. De Vries, *The Journal of Physical Chemistry B*, 2007, **111**, 7812-7824.
4. S. Kumar, J. M. Rosenberg, D. Bouzida, R. H. Swendsen and P. A. Kollman, *Journal of Computational Chemistry*, 1992, **13**, 1011-1021.
5. L. M. Souza, F. R. Souza, F. Reynaud and A. S. Pimentel, *Journal of Molecular Liquids*, 2020, 114132.
6. S. E. DeBolt and P. A. Kollman, *Journal of the American Chemical Society*, 1995, **117**, 5316-5340.
7. T. Taddese and P. Carbone, *The Journal of Physical Chemistry B*, 2017, **121**, 1601-1609.
8. S. J. Marrink, A. H. De Vries and A. E. Mark, *The Journal of Physical Chemistry B*, 2004, **108**, 750-760.
9. B. Jaidhan, P. S. Rao and A. Apparao, *Int. J. Comput. Sci. Inf. Technol*, 2014, **5**, 3525-3528.
10. G. Bussi, D. Donadio and M. Parrinello, *The Journal of Chemical Physics*, 2007, **126**, 014101.
11. H. J. Berendsen, J. v. Postma, W. F. van Gunsteren, A. DiNola and J. Haak, *The Journal of Chemical Physics*, 1984, **81**, 3684-3690.

12. M. Parrinello and A. Rahman, *Journal of Applied Physics*, 1981, **52**, 7182-7190.
13. S. I. Hossain, N. S. Gandhi, Z. E. Hughes and S. Saha, *Physical Chemistry Chemical Physics*, 2020, **22**, 15231.
14. C. Laing, S. Baoukina and D. P. Tieleman, *Physical Chemistry Chemical Physics*, 2009, **11**, 1916-1922.
15. F. Fornasier, L. M. Souza, F. R. Souza, F. Reynaud and A. S. Pimentel, *Journal of Chemical Information and Modeling*, 2020, **60**, 569-577.
16. M. Melo, H. Ingólfsson and S. Marrink, *The Journal of Chemical Physics*, 2015, **143**, 243152.
17. W. F. Van Gunsteren and H. J. Berendsen, *Molecular Simulation*, 1988, **1**, 173-185.
18. J. S. Hub, B. L. De Groot and D. Van Der Spoel, *Journal of Chemical Theory and Computation*, 2010, **6**, 3713-3720.
19. B. Efron, in *Breakthroughs in Statistics*, Springer, 1992, pp. 569-593.
20. I. V. Tetko, J. Gasteiger, R. Todeschini, A. Mauri, D. Livingstone, P. Ertl, V. A. Palyulin, E. V. Radchenko, N. S. Zefirov and A. S. Makarenko, *Journal of Computer-Aided Molecular Design*, 2005, **19**, 453-463.
21. Chem Axon. Chemicalize, https://chemicalize.com/welcome, (accessed April 22, 2021).
22. C. Hansch and A. Leo, *American Chemical Society*, 1995, **1**, 557-1037.
23. M. D. Daily, B. N. Olsen, P. H. Schlesinger, D. S. Ory and N. A. Baker, *Journal of Chemical Theory and Computation*, 2014, **10**, 2137-2150.
24. J. R. Espinosa, C. R. Wand, C. Vega, E. Sanz and D. Frenkel, *The Journal of Chemical Physics*, 2018, **149**, 224501.
25. S. Baluja and K. V. Chavda, *International Journal of Pharmaceutical, Chemical & Biological Sciences*, 2015, **5**.
26. D. Wishart, DrugBank, https://go.drugbank.com/drugs/DB00764, 2020).
27. N. R. Labiris and M. B. Dolovich, *British Journal of Clinical Pharmacology*, 2003, **56**, 588-599.
28. A. Fadl, J. Wang and Z. Zhang, *Inhalation Toxicology*, 2010, **22**, 601-609.
29. M. Dolovich, *Journal of Aerosol Medicine*, 1999, **12**, 9-17.
30. M. Ochs, J. R. Nyengaard, A. Jung, L. Knudsen, M. Voigt, T. Wahlers, J. Richter and H. J. G. Gundersen, *American Journal of Respiratory and Critical Care Medicine*, 2004, **169**, 120-124.
31. D. M. Hyde, N. Tyler, L. Putney, P. Singh and H. Gundersen, *The Anatomical Record Part A: Discoveries in Molecular, Cellular, and Evolutionary Biology: An Official Publication of the American Association of Anatomists*, 2004, **277**, 216-226.
32. Q. Hu, B. Jiao, X. Shi, R. P. Valle, Y. Y. Zuo and G. Hu, *Nanoscale*, 2015, **7**, 18025-18029.
33. L. S. Vermeer, B. L. De Groot, V. Réat, A. Milon and J. Czaplicki, *European Biophysics Journal*, 2007, **36**, 919-931.
34. L. Monticelli, S. K. Kandasamy, X. Periole, R. G. Larson, D. P. Tieleman and S.-J. Marrink, *Journal of Chemical Theory and Computation*, 2008, **4**, 819-834.